Astronomy & Astrophysics manuscript no.
(will be inserted by hand later)

The central region of M31 observed with *XMM-Newton*⋆

I. Group properties and diffuse emission

R. Shirey[1], R. Soria[2], K. Borozdin[3], J.P. Osborne[4], A. Tiengo[5], M. Guainazzi[5], C. Hayter[4], N. La Palombara[6], K. Mason[2], S. Molendi[6], F. Paerels[7], W. Pietsch[8], W. Priedhorsky[3], A.M. Read[8], M.G. Watson[4], and R.G. West[4]

[1] Department of Physics, University of California, Santa Barbara, Santa Barbara, CA 93106, USA
[2] Mullard Space Science Laboratory, University College London, Holmbury St. Mary, Dorking, Surrey RH5 6NT, UK
[3] NIS-2, Space and Remote Sensing Sciences, Los Alamos National Laboratory, Los Alamos, NM 87545, USA
[4] Department of Physics & Astronomy, University of Leicester, Leicester LE1 7RH, UK
[5] XMM-Newton SOC, VILSPA-ESA, Apartado 50727, 28080 Madrid, Spain
[6] Istituto di Fisica Cosmica "G.Occhialini", Via Bassini 15, 20133, Milano, Italy
[7] Columbia Astrophysics Laboratory, Columbia University, New York, NY 10027, USA
[8] Max Planck Institut für Extraterrestrische Physik, Giessenbachstraße, D-85741 Garching bei München, Germany

Received [date]; accepted [date]

Abstract. We present the results of a study based on an *XMM-Newton* Performance Verification observation of the central 30′ of the nearby spiral galaxy M31. In the 34-ks European Photon Imaging Camera (EPIC) exposure, we detect 116 sources down to a limiting luminosity of 6×10^{35} erg s^{-1} (0.3–12 keV, $d = 760$ kpc). The luminosity distribution of the sources detected with *XMM-Newton* flattens at luminosities below $\sim 2.5 \times 10^{37}$ erg s^{-1}. We make use of hardness ratios for the detected sources in order to distinguish between classes of objects such as super-soft sources and intrinsically hard or highly absorbed sources. We demonstrate that the spectrum of the unresolved emission in the bulge of M31 contains a soft excess which can be fitted with a ∼0.35-keV optically-thin thermal-plasma component clearly distinct from the composite point-source spectrum. We suggest that this may represent diffuse gas in the centre of M31, and we illustrate its extent in a wavelet-deconvolved image.

Key words. galaxies: individual: M31 – galaxies: spiral – galaxies: general – galaxies: ISM – X-rays: galaxies

1. Introduction

Being the closest spiral galaxy to our own, the Andromeda Galaxy (M31) is in many respects ideal for the study of X-ray emission in a galaxy similar to the Milky Way. The sources in M31 are observed at a nearly uniform distance, and, owing to the inclination of the galaxy (77°), they are viewed through a substantially lower absorption column than for sources in the Galactic plane.

In a recent review, van den Bergh (2000) reports a distance modulus to M31 of 24.4±0.1, corresponding to a distance of 760 kpc. We adopt this value in our analysis, and for consistency we scale to this distance when discussing published luminosities which assume a different distance.

Over 100 X-ray sources in M31 were detected with the *Einstein* observatory (Trinchieri and Fabbiano 1991; van Speybroeck et al. 1979). The brightest X-ray source in M31 was found to have a luminosity of $\sim 3\times10^{38}$ erg s^{-1}, approximately the Eddington luminosity for spherical accretion onto a 1.4 $M_\odot$ neutron star. For sources down to 2×10^{36} erg s^{-1}, the luminosity distribution was reported to be consistent with a single power law which, extrapolated to fainter levels, could fully account for the X-ray emission from the bulge of M31.

Primini, Forman, and Jones (1993) detected 86 X-ray sources in the central 34′ of M31 with the *ROSAT* HRI. They found a break in the luminosity distribution at $\sim 2\times10^{37}$ erg s^{-1}, below which the distribution of sources flattened. This flattening suggested that the detected population of X-ray sources could account for only ∼15–26%

Send offprint requests to: R. E. Shirey
⋆ Based on observations obtained with XMM-Newton, an ESA science mission with instruments and contributions directly funded by ESA Member States and the USA (NASA).
Correspondence to: shirey@xmmom.physics.ucsb.edu

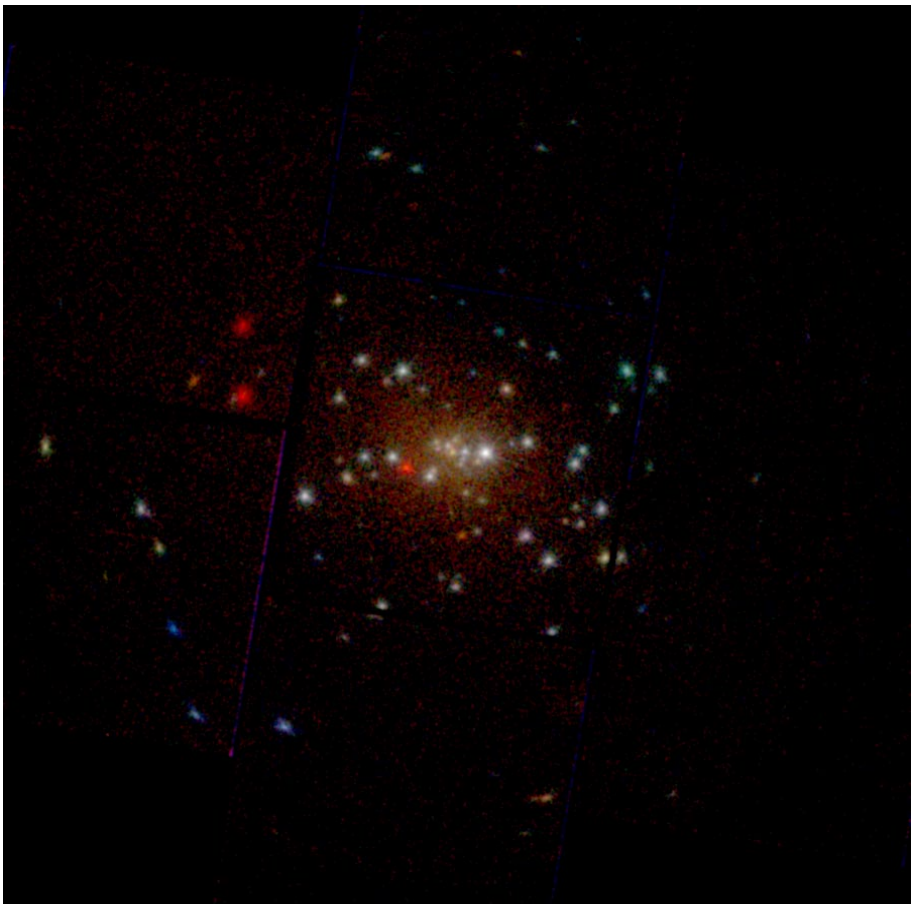

Fig. 1. Three-colour *XMM-Newton* EPIC MOS1 image of the central $30' \times 30'$ of M31. The red, green, and blue intensities correspond to logarithmically-scaled counts from energy bands of 0.3–0.8 keV, 0.8–2 keV, and 2–8 keV respectively. The image was constructed with $2''$ pixels and has been smoothed with a Gaussian of FWHM $4.4''$, approximately equal to that of the MOS1 PSF.

of the unresolved X-ray emission in M31. Contributions from known less-luminous populations of X-ray sources also could not fully account for the unresolved emission, suggesting that the remaining emission is truly diffuse or due to a new class of X-ray sources.

In an extensive, 6.3 deg^2, survey of M31 with the *ROSAT* PSPC, 396 X-ray sources were detected (Supper et al. 1997). However, only 22 of these sources were detected in the bulge region ($r < 5'$) due to the resolution of the PSPC.

In the first *Chandra* observation of M31, the nuclear source seen with *Einstein* and *ROSAT* was resolved into five sources (Garcia et al. 2000). One of these sources is located within $1''$ of the radio nucleus of M31 and exhibits an unusually soft X-ray spectrum, suggesting that it may be associated with the central super-massive black hole. A few more pairs of previously unresolved sources and a new transient were also detected within $30''$ of the nucleus.

M31 was selected as an *XMM-Newton* (Jansen et al. 2001) Performance Verification target in order to demonstrate the capabilities of *XMM* in performing spectral and timing studies in a field of point sources and extended emission. In this paper we focus on the group properties of the X-ray point sources in M31 as well as the diffuse emission. In a companion paper (Osborne et al. 2001, Paper II), we discuss the spectral and timing properties of individual X-ray sources in M31.

2. *XMM-Newton* Observations

The central region of M31 was observed with *XMM-Newton* on 2000 July 25. The observation was centred on the core of M31 ($\alpha = 00^h42^m43\overset{s}{.}0$, $\delta = +41°15'46.0''$ J2000), with a field of view of $30'$ in diameter for the three European Photon Imaging Camera (EPIC) instruments. Exposures of 34.8 ks were obtained with each of the two EPIC MOS instruments (Turner et al. 2001), and a 31.0-ks exposure was obtained with the EPIC PN (Strüder et al. 2001). All three EPIC instruments operated in full-window mode with the medium optical blocking filter. The two Reflection Grating Spectrometer (RGS) cameras (den Herder et al. 2001) each obtained 43-ks exposures (not discussed here). The Optical/UV Monitor Telescope (OM; Mason et al. 2001) filter wheel was set to the blocked position during this observation; however, UV and optical exposures with the OM are planned during upcoming Guaranteed-Time Observations of M31.

The background rate in the EPIC detectors was steady for the entire observation except for a background flare during the final 5 ks. Data from this background flare are excluded from the image in Figure 1 and from our analysis of extended regions; however, we have found that they do not significantly affect the spectra of individual

point sources. Therefore, the entire data-set was used for the extraction of discrete sources.

We used the *XMM-Newton* Science Analysis System (versions from 2000 Sept.) to reduce the EPIC data to calibrated event lists, produce images, and extract spectra. We used a combination of SAS programs and external software to further analyse the data. In this paper, we concentrate on data from MOS1 but we have used a sample of data from MOS2 and PN to confirm the consistency of our results. Slight differences in the locations of sources on the outer MOS1 CCDs relative to MOS2 and PN indicate that the calibration of chip boundaries must be refined. We used the response matrix `mos1_medium_all_v3.17_15_tel4.rsp` for fitting MOS1 spectra; we checked that our results do not change significantly if the more recent response matrix `mos1_medium_all_qe17_rmf3_tel5_15.rsp` (2000 Oct.) is used.

3. EPIC Images

The EPIC images of the central 30′ of M31 (e.g., the MOS1 image in Figure 1) contain more than 100 discrete X-ray sources as well as unresolved emission near the centre. The images show four very soft (red) sources: two of them were identified by Kahabka (1999) as candidate super-soft sources (SSS), based on a wider *ROSAT* PSPC hardness-ratio criteria than the original sample of SSS identified by Supper et al. (1997); one is coincident with a super-nova remnant; the fourth one is an unidentified source detected with the *ROSAT* HRI (Primini et al. 1993). Several very hard (blue) sources are also present. The nature of these extreme-colour objects is discussed below in the context of the point-source group properties.

4. Discrete X-ray sources

4.1. Source Detection

Sources were detected with the IRAF routine DAOPHOT (Stetson 1987); the SAS produced similar results. We determined the point spread function (PSF) from the brightest sources in our image rather than from calibration models, and we used the measured PSF to fit source intensities. The FWHM of the PSF is a function of energy and distance from the image centre; for the core region ($r < 5'$, $\sim$1.1 kpc), where most of the sources are found, $FWHM = 4''$–$7''$. It is more difficult to determine the PSF for sources at $\gtrsim 10'$ from the centre. For a few of these off-axis sources, we compared the count rate found with the PSF fitting routine with the rate obtained by considering a $30''$ source circle and a $15''$ sky annulus. We find that the count rates obtained with the two methods are similar. We also correct the count rates of all the sources for the vignetting of the XMM telescope, based on the Current Calibration Files provided with the SAS.

We detect 116 discrete sources above a 5σ threshold. Two sources previously identified as foreground or background objects (*ROSAT* HRI sources 9 and 82 Primini et al. 1993) have been excluded from the analysis below. In addition, three sources at or near the nucleus have been resolved into two or more sources with *Chandra* (Garcia et al. 2000) and are thus also excluded from our discussion of the luminosity distribution.

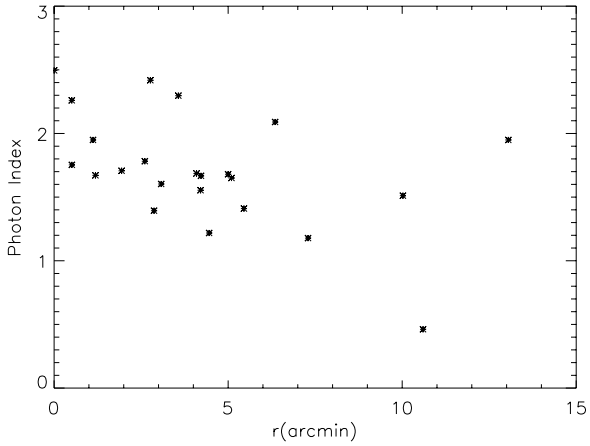

Fig. 2. Photon index versus distance from the nucleus (r) for 23 bright sources with $>$ 500 counts in the first 30 ks of the MOS1 observation. (Two super-soft sources have been excluded from this plot, as well as two sources not belonging to M31.)

4.2. Spectral Characterisation

We have fitted simple absorbed power-law models to the spectra of the 23 brightest point sources (those with more than 500 counts above the background in the first 30 ks of observation). We present more detailed spectral fits of selected sources in Paper II. In order to obtain the spectra of the bright sources, we used an extraction radius of $\sim 15''$; we subtracted a background extracted from an annulus at the same distance from the galactic centre as the source and from which the point sources have been removed. The resulting spectra were fitted with an absorbed power-law model, with the column density fixed at $N_H = 1 \times 10^{21}$ cm^{-2}. Figure 2 shows the fitted photon indices plotted versus the distance of each source from the M31 nucleus. We note that the hardest sources tend to be outside the central few arcminutes of the galaxy.

In order to characterise the gross spectral properties of all the detected sources, including those for which we do not have enough counts for spectral fitting, we derived source counts in soft (S) and hard (H) energy bands of 0.3–2.0 keV and 2.0–12 keV respectively, and we constructed hardness ratios defined as $(H - S)/(H + S)$. In Figure 3, we show the hardness ratio versus total count rates of all the 116 sources detected in EPIC MOS1. Thirteen sources detected only in the soft band are plotted with a hardness ratio $= -1$. Among this group of very soft sources, three have an estimated emitted luminosity $\gtrsim 10^{37}$ erg s^{-1} (see Section 4.3); as mentioned above, two of them are super-

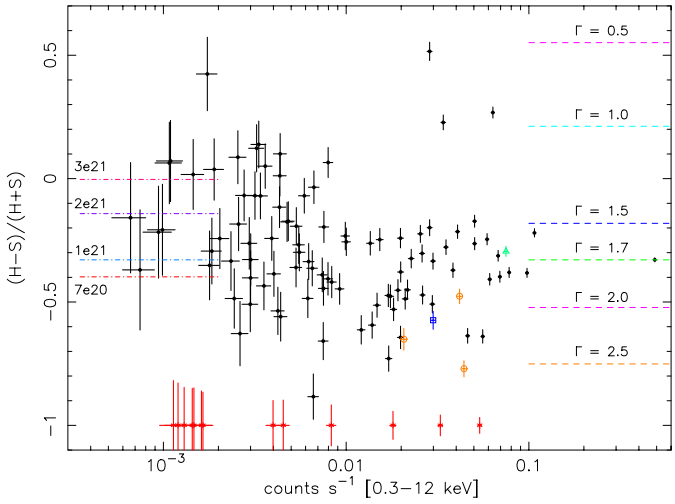

Fig. 3. Hardness ratio of the discrete sources detected in M31, versus the total count rate in the 0.3–12 keV band. S is the count rate in the 0.3–2 keV band; H is the count rate in the 2–12 keV band. See the text for an explanation of plot symbols.

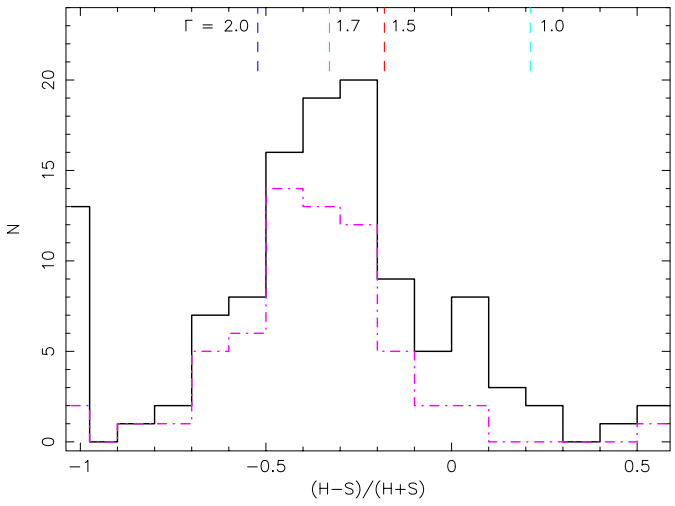

Fig. 4. Hardness distribution of all detected sources (solid line) and sources at $r < 5'$ (dash-dotted line) compared with expected hardness ratio for various values of the photon index Γ, at fixed $N_H = 1{\times}10^{21}$ cm^{-2}. Sources plotted with hardness $= -1$ are not detected in the hard band.

soft sources, and the third one is identified with an SNR. The three bright, blue sources in Figure 1 all have hardness ratios significantly larger than the other sources in Figure 3. We show in Paper II that these sources are intrinsically hard, rather than highly absorbed. In Figure 3, we have included three core sources resolved with *Chandra*, plotted here as open circles. The softest (and brightest) of these three unresolved *XMM-Newton* sources contains the true nucleus CXO J004244.2+411608 (Garcia et al. 2000); its hardness ratio confirms that the spectrum of the nucleus is very soft. The open triangle marks the bright transient found with *Chandra* (Garcia et al. 2000). The open square marks a bright new transient source we detected with *XMM-Newton* (Paper II).

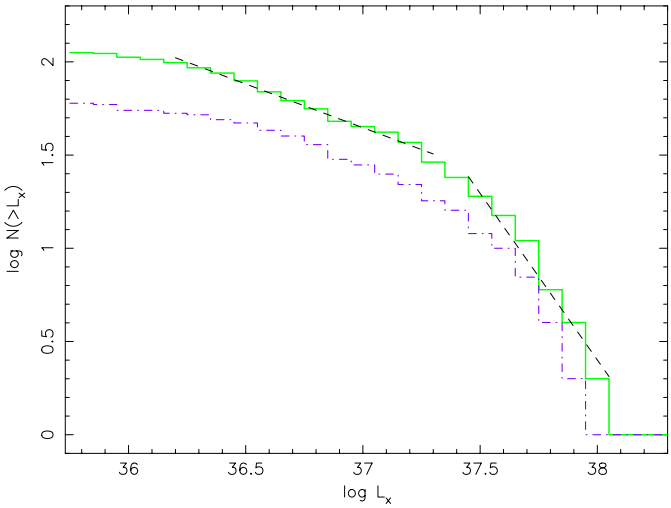

Fig. 5. Integral luminosity distribution of X-ray sources detected with *XMM-Newton* at 0.3–12 keV over the full 30′ EPIC-MOS field of view (solid line) and in the core of M31 ($r < 5'$ from the centre; dashed-dotted line). L_x is in units of erg s^{-1}. The indices of the power-law fits to the high- and low-luminosity parts of the total distribution are −1.79 and −0.47 respectively (see text for details). The unabsorbed luminosity of the ∼ 20 brightest sources has been directly determined with spectral fits, while the values for all other sources are based on a count rate to luminosity conversion factor of 1 count s^{-1} $= 8.9 \times 10^{38}$ erg s^{-1}.

On the right-hand side of Figure 3, we have marked with dashed lines the expected hardness ratios of sources characterised by a pure power-law spectrum of various photon indices (from 0.5 to 2.5) for a fixed column density $N_H = 1{\times}10^{21}$. On the left-hand side, we have marked with dash-dotted lines the expected hardness ratios for various column densities $N_H = 7{\times}10^{20}$–$3{\times}10^{21}$ cm^{-2}, for a fixed photon index 1.7. The majority of sources we detect have hard and soft intensities consistent with a power law of photon index 1.0–2.5 and column densities $N_H = 7{\times}10^{20}$–$3{\times}10^{21}$ cm^{-2}. Histograms of the hardness ratio distribution for all sources and for those sources within 5′ of the M31 nucleus are shown in Figure 4. The hardness ratio plots justify our choice of a power-law spectral model with photon index 1.7 and $N_H = 1{\times}10^{21}$ for our conversion from count rate to luminosity (see Section 4.3).

4.3. Luminosity Distribution

We convert from count rates to unabsorbed luminosities in the 0.3–12 keV range by using an absorbed power-law model with $N_{\rm H} = 1{\times}10^{21}$ cm^{-2} and $\Gamma = 1.7$, for a distance of 760 kpc. This gives a count rate to luminosity conversion factor of 1 count s^{-1} $= 8.9 \times 10^{38}$ erg s^{-1}. If we take an average of the 23 brightest sources (see Figure 2), we obtain a conversion factor of 1 count s^{-1} $= (8.4 \pm 1.0) \times 10^{38}$ erg s^{-1}, consistent with the previous model. For the brightest source only, a conversion factor of 1 count s^{-1} $= 9.1 \times 10^{38}$ erg s^{-1} is obtained. The observed spread in the values of the conversion factor for sources

with different spectral characteristics gives us an estimate of the error ($\approx 10\%$) in the luminosity of faint sources for which no spectral fit is available. The limiting sensitivity of our sample is $\approx 6 \times 10^{35}$ erg s^{-1}.

The cumulative luminosity distribution for all the X-ray sources in the EPIC MOS field of view is shown in Figure 5. We also determined a luminosity distribution for the 60 sources detected in core of M31 ($r < 5'$ from the centre); we plot it in Figure 5 as a dash-dotted line. Our data show a flattening of the luminosity distribution for $L_{\rm x} \lesssim 2.5 \times 10^{37}$ erg s^{-1}. We fitted the low- and high-luminosity sections of the total distribution with simple power laws. For $36.2 \leq \log L_{\rm x} < 37.4$, we obtain a power-law index of -0.47 ± 0.03; for $37.4 \leq \log L_{\rm x} < 38.1$, the power-law index is -1.79 ± 0.26. For the core source distribution, the power-law indices are -0.43 ± 0.04 and -1.77 ± 0.35 respectively. Thus, we find no significant difference in the shape of the distribution for sources in the core compared with the distribution for all the sources out to $r \approx 15'$. These results are in agreement with the luminosity distribution found by Primini et al. (1993) and Supper et al. (1997).

Based on *Chandra* deep field results (Giacconi et al. 2000), we estimate that at the faint end of the luminosity distribution, at $\log L_{\rm x} = 36.2$, we might expect 10–20 background AGN in the field of view. We would also expect about half that number of foreground K and M stars (following Supper et al. 1997). Correction for the contribution of such foreground/background objects would further flatten the faint end of the full-field-of-view distribution but would not significantly affect the brighter portion of the distribution. In the much smaller core region ($r < 5'$), we estimate the contribution of background AGN or foreground stars to the luminosity distribution above $\log L_{\rm x} = 36.2$ to be minimal, i.e., in the core we expect $\sim$ 1–3 AGN and 0 or 1 stars brighter than that level.

The 0.3–12 keV observed luminosity of the brightest X-ray source in our sample is $L_{\rm x} = (3.9 \pm 0.2) \times 10^{38}$ erg s^{-1}, corresponding to an emitted luminosity of $(4.5 \pm 0.2) \times 10^{38}$ erg s^{-1} for the fitted spectral model and column density. For a comparison with earlier *ROSAT* observations (Primini et al. 1993; Supper et al. 1997), this corresponds to an emitted luminosity of $(2.6 \pm 0.1) \times 10^{38}$ erg s^{-1} in the 0.1–2.4 keV band, and of $(2.9 \pm 0.1) \times 10^{38}$ erg s^{-1} in the 0.2–4.0 keV band. These values are in agreement with the *ROSAT* results, when we take into account our different choice of spectral model, column density and distance to M31.

We determine an integrated 0.3–12 keV emitted luminosity $L_{\rm x} = (2.2 \pm 0.2) \times 10^{39}$ erg s^{-1} for the region at $r < 5'$. The background was extracted from regions at $r > 7'$, excluding detected sources. The result is insensitive to the exact model used for the spectral fitting and the region selected for the background. The 0.1–2.4 keV emitted luminosity $L_{\rm x} = (1.35 \pm 0.15) \times 10^{39}$ erg s^{-1}, in agreement with the *ROSAT* results (Supper et al. 1997). The total 0.3–12 keV contribution of the discrete sources we detected in the core, correcting for an estimated 20% of the counts being in the PSF wings, is $L_{\rm x,s} \approx (2.0 \pm 0.1) \times 10^{39}$ erg s^{-1}, i.e., they account for $\sim (90 \pm 10)\%$ of the total X-ray emission in the core. If we extrapolate the observed luminosity distribution of the core to a lower limit of 10^{34} erg s^{-1}, we obtain only a small additional contribution of $\lesssim 10^{38}$ erg s^{-1} based on the power-law index fitted to the distribution at $36.2 \leq \log L_{\rm x} < 37.4$, or even less if the flattening below $\log L_{\rm x} \sim 36$ continues to fainter levels.

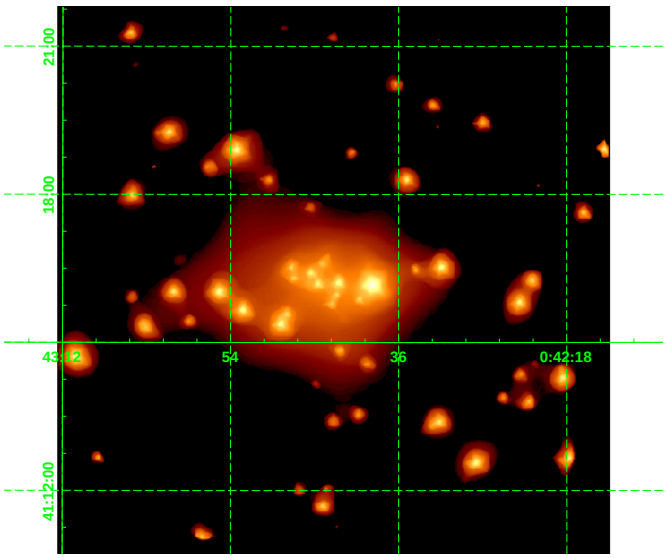

Fig. 6. Wavelet-deconvolved EPIC MOS1 image of the central $10'$ of M31, showing diffuse emission as well as numerous point sources.

5. Diffuse emission

As mentioned in the Introduction, *ROSAT* results suggested the presence of diffuse X-ray emission in the core of M31 (Primini et al. 1993). Recently, it was reported that *Chandra*, in spite of its excellent imaging capabilities, does not resolve all the soft X-ray emission from the central part of M31 into individual sources (Garcia et al. 2000). The extent of the unresolved X-ray emission in the *XMM-Newton* observation is illustrated by a wavelet-deconvolved image in Figure 6. In order to determine the nature of the unresolved emission seen in the image, we performed spectral analysis of several regions in the central part of M31.

We first extracted the composite spectrum of 44 bright point sources detected within $5'$ of the nucleus. Trying to maximise the relative contribution of point sources in this spectrum, we collected only data within small circles around each source, with radii of $10''$–$30''$ ($\sim$ 60–85% encircled energy fraction) depending on the source brightness (smaller radii for fainter sources). We then collected a spectrum from areas where significant unresolved emission is present and no point sources were detected. We collected the background spectrum from the same MOS chip, but outside its central region, in areas where no point

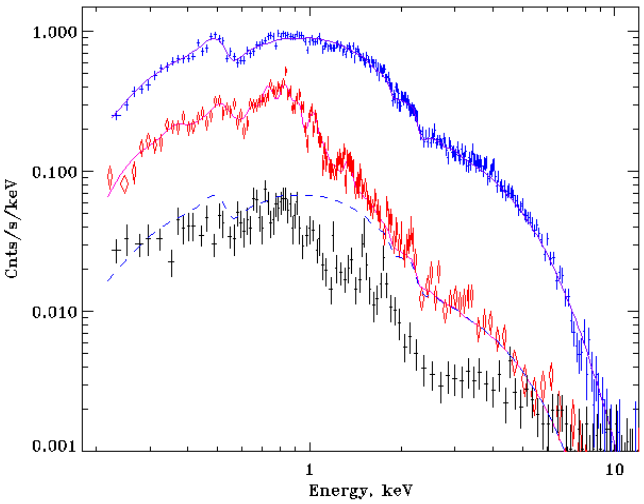

Fig. 7. EPIC MOS1 spectra collected from different regions of the M31 bulge. Blue crosses represent the sum of 44 bright sources located within 5′ from the centre; the violet line is a fit of this spectrum with a single power-law model. The spectrum of unresolved emission is shown by red diamonds; the blue dashed line shows contribution of a power-law component with the same slope as the top curve. The need for an additional thermal plasma component associated with the diffuse bulge emission is clearly seen. The pink solid line is a fit of the unresolved-emission spectrum with a two-component model. Black crosses below show the background, collected in the outer parts of the same MOS chip. All three spectra are normalised to the same area. The two upper spectra have been background-subtracted using the bottom background spectrum scaled to the appropriate area. See the text for details of the analysis and model parameters.

sources were detected. We cannot exclude a small contamination of the background by unresolved point sources and faint diffuse emission; however, since the background is much fainter than the point-source and unresolved emission at all but the highest energies (Figure 7), this is not likely to be a significant source of error. The shape of the background spectrum is not significantly affected by vignetting, because, for a given off-axis angle on the central chip, the vignetting function varies with energy by no more than $\sim 6\%$ for $E \lesssim 6$ keV. The vignetting function at different off-axis angles on the central chip is also relatively flat, decreasing by only $\sim$15% from the centre to 5′ off axis and by a total of $\sim$25% at 7′ off axis.

We scaled the spectra of the unresolved emission and of the background to the area of the point-source spectrum. We show the background-subtracted point-source and unresolved spectra, along with the background itself, in Figure 7. The point-source spectrum is well fitted with a power law of photon index 1.82 ± 0.03 and absorption column density $N_H = (6.7 \pm 0.4) \times 10^{20}$ cm^{-2}. This spectrum is typical of low-mass X-ray binaries (LMXBs) and the column density is close to the Galactic column along the line of sight to M31. In contrast, the spectrum of the unresolved emission cannot be fitted with a single power-law component. Above $\sim$2 keV, a power-law component of the same slope as the point-source spectrum is dominant, but a significant soft excess is clearly present below this energy. This soft excess can be fitted with an additional component from an optically-thin thermal plasma (MEKAL) with $kT \sim 0.35$ keV.

Based on the portion of the PSF that fell outside our exclusion region around each point source, we conclude that the power-law component in the spectrum of the unresolved emission is mostly due to point-source counts in the wings of the PSF. A further contribution to this component may come from faint LMXBs below our detection limit. An accurate determination of the relative contribution of PSF wings, unresolved LMXBs, background, and any other component to the hard portion of the unresolved emission will require further knowledge of the instrument performance. We thus defer this task to a future work.

We now turn our attention to the soft portion of the unresolved emission. The fraction of encircled energy inside a chosen angular radius falls with energy for *XMM*, so that the spectrum of the PSF wings should be harder than the extracted point-source spectrum; thus, the PSF wings cannot contribute to the soft excess in the unresolved emission. Moreover, Figure 7 shows that the contribution of the background in this spectral region is much smaller than the soft excess. Therefore, the soft excess and its thermal-plasma spectrum cannot be explained by instrumental or background effects.

What is the physical nature of this component? It was suggested by Irwin & Bregman (1999) that LMXBs could contribute to the soft excess. However, we have not detected a significant soft component in the LMXB-dominated point-source spectrum. Furthermore, we have shown in Fig. 3 that the fainter sources we detect have a similar or higher hardness ratio than most of the brighter sources. Therefore, we see no evidence that LMXBs might significantly contribute to the soft spectral excess.

We cannot exclude that a population of faint point sources with soft X-ray spectra, different from the population of our detected bright sources, may be responsible for part or all of the soft X-ray excess. However, because the soft excess in the unresolved emission spectrum is well fitted with a thin thermal plasma model with significant line emission, we favour the interpretation of the soft excess as truly diffuse emission from hot, optically-thin plasma.

We fit the background-subtracted spectrum of the total emission within $r < 5'$ using the thermal-plasma plus power-law model and found that the thermal component contributes $\sim$10% of the total unabsorbed spectral flux (0.3–12 keV). We accept this spectrally-determined value as our best estimate of the diffuse-emission contribution to the X-ray luminosity of the bulge of M31. This value is also consistent with our estimate based the discrete source distribution (Section 4.3). We leave a more precise determination of the relative contribution of diffuse emission to the total X-ray flux to a future work when calibration details are more secure.

6. Conclusions

Using *XMM-Newton* data, we have confirmed that the X-ray emission from the bulge of M31 is dominated by bright point-like sources, most of which are likely to be low-mass X-ray binaries. For sources in the central region of M31, we have confirmed that the luminosity distribution is flatter toward lower luminosities (Primini et al. 1993). The steepening of the luminosity distribution above 2.5×10^{37}erg s^{-1} is indicative of a lack of bright sources in M31 (cf. the source distribution in M33, Long et al. 1996). Only two sources in our sample have a 0.3–12 keV unabsorbed luminosity $\geq 10^{38}$erg s^{-1}.

As in previous observations with *Einstein* and *ROSAT* (Trinchieri and Fabbiano 1991; Primini et al. 1993), significant unresolved emission was found to contribute to the total emission of the bulge. The flattening of the luminosity distribution for fainter sources means that an extrapolation of the detected population of point sources at lower energies cannot account for the total core emission of M31.

A soft excess in the spectrum of the M31 bulge was previously reported in *ROSAT* and *BeppoSAX* observations (Irwin and Bregman 1999; Trinchieri et al. 1999). Our analysis of the *XMM-Newton* data shows that the soft component in the spectrum of the bulge is associated with unresolved emission; this confirms the results of Borozdin and Priedhorsky (2000) based on *ROSAT* data.

More importantly, our *XMM-Newton* study has revealed for the first time that while the integrated spectrum of point-like sources is featureless, the spectrum of the unresolved emission shows multiple emission lines typically found in the spectrum of hot, optically thin plasma. Therefore, we suggest that the second significant source of X-ray emission in the bulge is truly diffuse gas with an effective temperature ∼0.35 keV. The contribution of this gas to the total unabsorbed X-ray luminosity is estimated to be ∼10% in 0.3–12 keV band (corresponding to $\approx 2 \times 10^{38}$erg s^{-1}), but more than 20% in the *ROSAT* band (0.1–2.4 keV). The significance of this result goes far beyond the case of M31, because the bulge of this galaxy is often considered as a prototype for the population of early-type X-ray galaxies. For example, Sarazin et al. (2000) recently reported that, according to *Chandra* observations, 23% of X-ray emission from NGC 4697 is emitted by interstellar gas, contrary to their previous expectations (Irwin et al. 2000).

Two more *XMM-Newton* observations of the central region of M31 are scheduled as part of the Guaranteed-Time program, as are observations of five additional fields along the disk of M31. These will allow us to reach fainter flux levels in the bulge and to study the populations of X-ray sources in different parts of the M31 galaxy.

Acknowledgements. We thank all the members of the *XMM-Newton* teams for their work building, operating, and calibrating the powerful suite of instruments on-board.

References

Borozdin, K. N. and Priedhorsky, W. C., 2000, ApJL, in press
den Herder, J. W. et al., 2001, A&A 365, (this issue)
Garcia, M. et al., 2000, abstract
Garcia, M. R., Murray, S. S., Primini, F. A., Forman, W. R., McClintock, J. E., and Jones, C., 2000, ApJ 537, L23
Giacconi, R. et al., 2000, ApJ, submitted (astro-ph/0007240)
Irwin, J. A. and Bregman, J. N., 1999, ApJ 527, 125
Irwin, J. A., Sarazin, C. L., and Bregman, J. N., 2000, ApJ, in press (astro-ph/0007408)
Jansen, F. et al., 2001, A&A 365, (this issue)
Kahabka, P., 1999, A&A 344, 459
Mason, K. et al., 2001, A&A 365, (this issue)
Osborne, J. et al., 2001, in preparation, (Paper II)
Primini, F. A., Forman, W., and Jones, C., 1993, ApJ 410, 615
Stetson, P. B., 1987, PASP 99, 191
Strüder, L. et al., 2001, A&A 365, (this issue)
Supper, R., Hasinger, G., Pietsch, W., Truemper, J., Jain, A., Magnier, E. A., Lewin, W. H. G., and van Paradijs, J., 1997, A&A 317, 328
Trinchieri, G. and Fabbiano, G., 1991, ApJ 382, 82
Trinchieri, G., Israel, G. L., Chiappetti, L., Belloni, T., Stella, L., Primini, F., Fabbiano, P., and Pietsch, W., 1999, A&A 348, 43
Turner, M. et al., 2001, A&A 365, (this issue)
van den Bergh, S., 2000, The Galaxies of the Local Group, Cambridge University Press, Cambridge
van Speybroeck, L., Epstein, A., Forman, W., Giacconi, R., Jones, C., Liller, W., and Smarr, L., 1979, ApJ 234, L45